Statics and dynamics of flux line lattices of high-T_c superconductors

1992 J. Phys.: Condens. Matter 4 445

(http://iopscience.iop.org/0953-8984/4/2/013)

J. Phys.: Condens. Matter 4 (1992) 445–459. Printed in the UK

Statics and dynamics of flux line lattices of high-T_c superconductors

Hong-ru Ma and S T Chui
Bartol Research Institute, University of Delaware, Newark, DE 19716, USA

Received 29 July 1991

Abstract. We investigate the energy, elastic modulus and normal modes of oscillation of flux line lattices. To deal with the long range nature of the flux line potential, the Ewald sum technique was used. The dependence of the normal modes as a function of the transverse wavevector in the 2D hexagonal Brillouin zone and the z wavevector k_z is discussed in detail. We found two normal modes corresponding to the shear and the compression of the lattice. The frequencies of these two are usually very different from each other. Because of the long range nature of the potential, the compressive mode behaves like a plasma oscillation. At zero momentum the exciations are gapless, because the potentially is exponential in character at large distances. At a finite z wavevector we found that the transverse frequencies drop off rapidly as the transverse wavevector is increased. Our elastic moduli are compared with those computed using a continuum approximation by Sudbø and co-workers. Quantitative differences are found in the low field, small k region as well as the high field, large k region.

1. Introduction

For a sufficiently strong magnetic field, flux lines penetrate type-II superconductors and form a lattice. To calculate the physical properties of the flux lattice, it is often necessary to perform averages over the normal modes of the system. It is thus important to understand the elastic coefficients and the normal modes in detail.

The interaction energy U of flux lines of arbitrary shape was given recently in terms of the penetration depths along the ab plane and the z direction, λ_{ab} and λ_z, by Sudbø and Brandt [1] based on the London equations as

$$U = \frac{\Phi\ 2}{8\pi}\sum_{m,n}\int \mathrm{d}l_i\ \mathrm{d}l_j\ \bar{V}_{ij}(\boldsymbol{r}_m - \boldsymbol{r}_n)$$

where

$$\bar{V}_{ij}(\boldsymbol{r}) = \int \frac{\mathrm{d}\ 3k}{(2\pi)\ 3} V_{ij}(\boldsymbol{k})\mathrm{e}^{\mathrm{i}\boldsymbol{k}\cdot\boldsymbol{r}}.$$

Here $V_{ij} = V^a_{ij} - V^b_{ij}$; $V^a_{ij}(\boldsymbol{k}) = V_0\delta_{ij}$, $V^b_{ij}(\boldsymbol{k}) = (V_0 q_i q_j \Lambda_2)/(1 + \Lambda_1 k^2 + \Lambda_2 q^2)$, $V_0 = 1/(1+\Lambda_1 k^2)$. The wavevector $\boldsymbol{q}$ lies in the ab plane of the crystal and is given by $\boldsymbol{q} = \boldsymbol{k}\times\hat{c}$ where c is a unit vector along the c axis of the crystal. $\Lambda_1 = \lambda^2_{ab}$, $\Lambda_2 = \lambda^2_c - \lambda^2_{ab}$. To incorporate the effect of the core structures of flux lines a cut-off factor of $\exp(-\zeta k_\perp^2)$ was introduced into V. Here $\zeta = (\xi/2\pi)^2$ where ξ is the coherence length.

For a flux lattice, the physical properties involve a sum over the reciprocal lattice vectors Q of the lattice. Because the penetration depth is much larger than the lattice spacing of the flux lattice, the interaction between flux lines is long range in nature. We have thus generalized the Ewald sum technique to the present calculation. This consists of splitting the sum over Q into two rapidly convergent sum in momentum and position space. We verify the accuracy of the calculation by varying the Ewald cut-off parameter and making sure that the final result is unchanged. Our result is summarized in (8) below.

This paper is organized as follows. The total energy of the lattice, the normal modes and the elastic coefficients are discussed in the first three sections for YBCO and BSCCO. The mathematical details of the Ewald sum is discussed in the next section. We conclude in the last section.

2. Energy

The energy of a periodic array of straight flux lines is

$$U/NL = \frac{B^2}{8\pi}\sum_{Q} V_{zz}(Q). \tag{1}$$

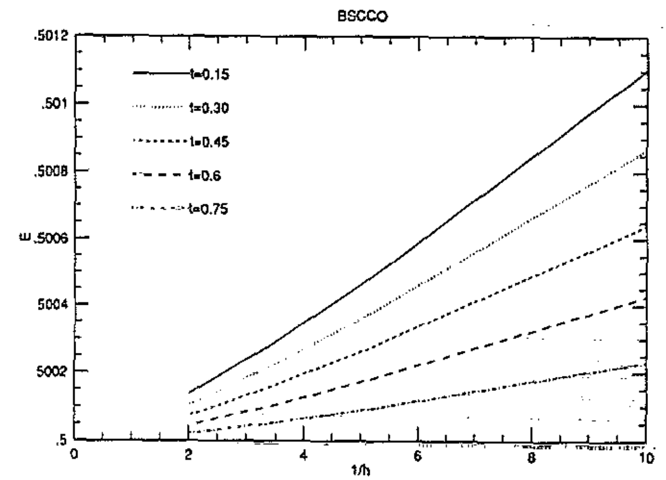

Figure 1. Energy per particle (in units of $B^2/4\pi$) of triangular BSCCO flux lattices as a function of the inverse magnetic field (in units of B_{c2}) for different reduced temperatures $t = T/T_c$.

The sum runs over all reciprocal lattice vectors Q at a given inclination of B with respect to $\hat{c}$. The basis vectors of the undistorted equilibrium lattice with B tilted by an arbitrary angle Θ away from the $\hat{c}$-axis are given by [1] $a_1 = C\hat{x}$ and $a_2 = C(\gamma\hat{x} + \sqrt{3}\hat{y}/\gamma)/2$, where $\gamma^4 = (M/M_z)\sin^2\Theta + \cos^2\Theta$ and $C^2 = 2\Phi_0/\sqrt{3}B$. The corresponding reciprocal lattice vectors are given by $Q_{mn} = nQ_1 + mQ_2$, with m, n integers and $Q_1 = (2\pi/C)(\hat{x}/\gamma - \gamma\hat{y}/\sqrt{3}), Q_2 = (2\pi/C)(2\gamma/\sqrt{3})\hat{y}$.

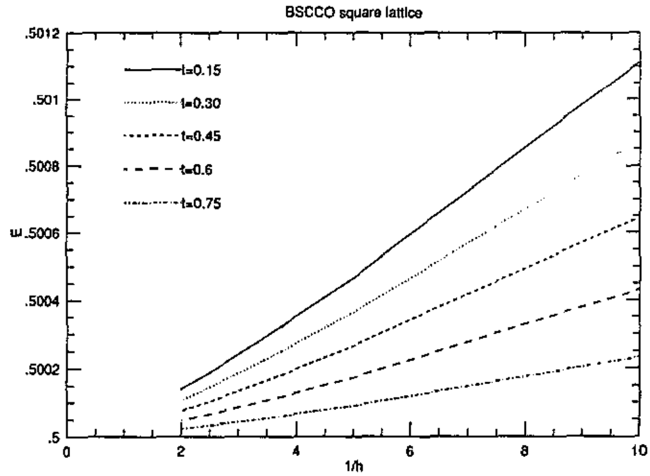

Figure 2. As figure 1, but for square BSCCO flux lattices.

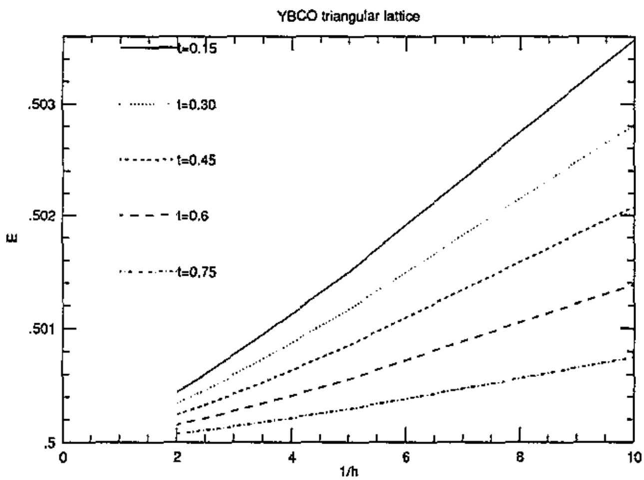

Figure 3. As figure 1, but for triangular YBCO flux lattices.

For simplicity, we consider in the following the case $B||c$, it is straightforward to generalize the calculation to the general case. In the following, we shall use units such that the flux lattice constant is equal to 1.

We have evaluated the energies of square and triangular lattices for BSCCO and YBC. For YBCO and BSCCO, we have used mass ratios, M_z/M of 25 and 625 and GL parameters κ of 50 and 90 respectively. We found the energy of the square lattices to be higher. For example, for BSCCO for $B/B_{c2} = 0.1$ and $t = T/T_c = 0.1$, the square lattice energy per particle is 0.501 190 5599 in units of $B^2/4\pi$ whereas that for the triangular lattice is 0.501 184 680 5008. We show in figures 1–4 the energy per particle as a function of the inverse reduced magnetic field for different reduced temperatures for the triangular and square lattices for BSCCO and YBCO respectively. As one can see, the dependence on the magnetic field is close to but not exactly an inverse dependence.

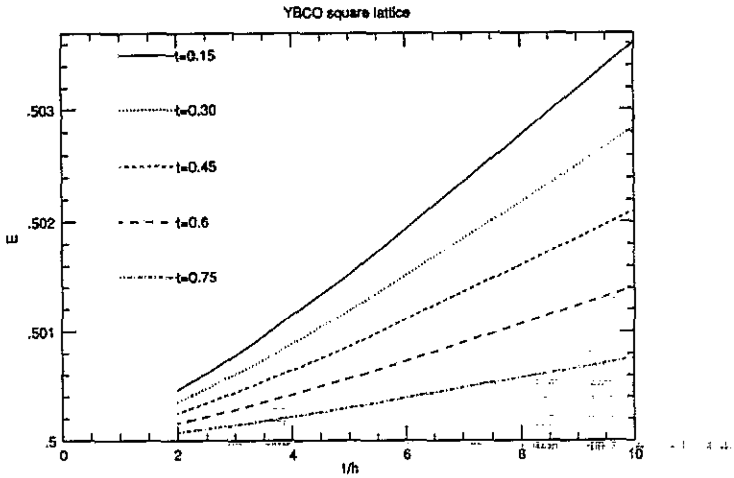

Figure 4. As figure 1, but for square YBCO flux lattices.

3. Normal modes

The harmonic energy U_0 of vibration can be written in terms of the deviations s of the flux lines from the lattice positions as

$$U_0 = \frac{1}{2}\sum_{\boldsymbol{k}} \Phi_{\alpha\beta}(\boldsymbol{k}) s_\alpha(-\boldsymbol{k}) s_\beta(\boldsymbol{k}) \tag{2}$$

where the dynamical matrix is

$$\Phi_{\alpha\beta}(k) = \frac{B^2}{4\pi}\sum_{Q}[k_z^2 V_{\alpha\beta}(k+Q) + (k+Q)_\alpha(k+Q)_\beta V_{zz}(k+Q) - Q_\alpha Q_\beta V_{zz}(Q)] \tag{3}$$

where $(\alpha, \beta, \ldots) \in (x, y)$.

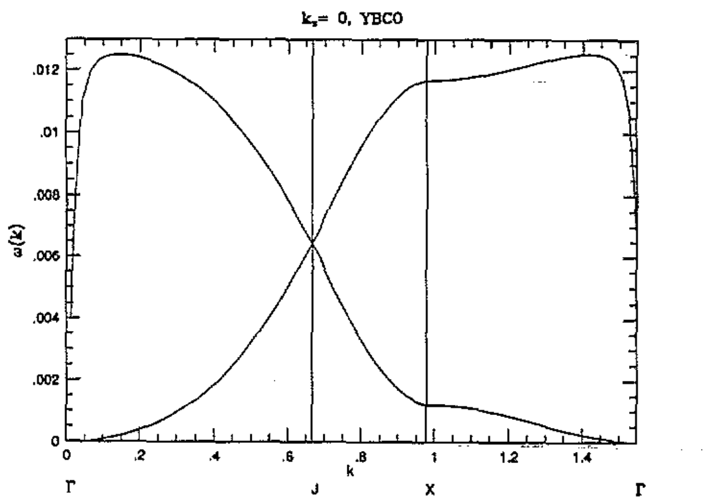

Figure 5. The normal mode frequencies (in units of $B^2/4\pi$) along symmetry directions in the 2D hexagonal Brillouin zone at $k_z = 0$ for YBCO.

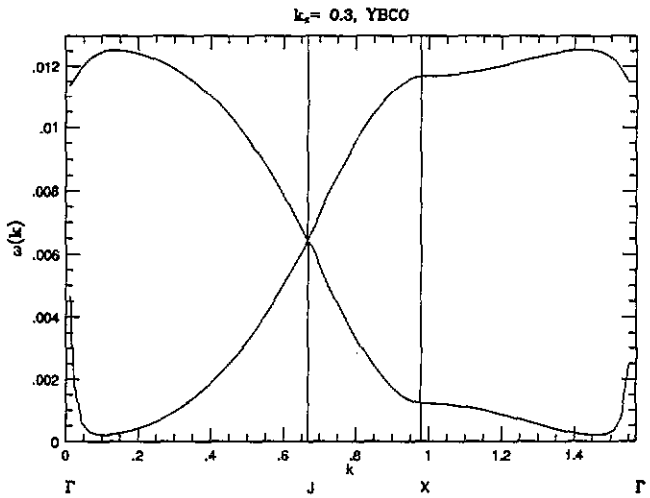

Figure 6. As figure 5, but at $k_z = 0.3$.

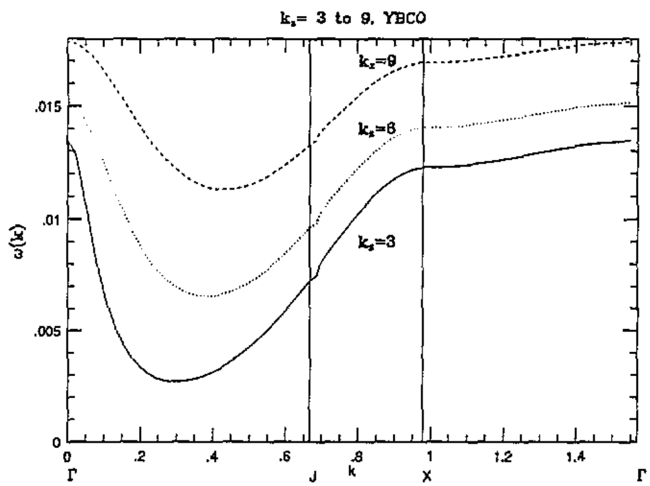

Figure 7. As figure 5, but at $k_z = 3, 6, 9$.

The dynamical matrix is evaluated with the Ewald sum technique, the details of which are discussed in section 5. For any given wavevector, the normal modes are obtained by diagonalizating the 2×2 matrices $\Phi_{\alpha\beta}(k)$. The frequencies are functions of the magnetic field and temperature. As a representative example, we first focus our discussion for a field stength of 1 T and reduced temperature of 0.8. The eigenvalues ω of this matrix along symmetry directions of the 2D hexagonal Brillouin zone for two values of the z wavevector k_z (0 and 0.3) for YBCO are shown in figures 5, 6 and 7 in units of $B^2/4\pi$. For $k_z = 0$, the very different slopes of the two modes at small wavevectors reflect the difference in magnitude between the elastic modulus c_{66} and c_{11} and is a manifestation of the long range of the potential and the near incompressibility of the system. For a finite k_z, the normal frequencies is finite at $k_\perp = 0$, and of magnitude $c_{44}k_z^2$. More interesting is the rapid decrease of the shear mode frequency as the transverse wavevector is increased. This comes about because $V^a_{\alpha\beta}$ nearly cancels $V^b_{\alpha\beta}$ for $q > q_c = 1/\sqrt{\Lambda_2}$. As k_z is further increased, V^b is decreased and the shear mode eigenvalue is no longer small. This is illustrated in figure 7 for $k_z = 3$, 6 and 9. A typical scan of the 2D dispersion for BSCCO for $k_z = 0.3$ is shown in figure 8. Because Λ_2 is now much bigger, the rapid drop of the transverse mode occurs over a much narrower wavevector range.

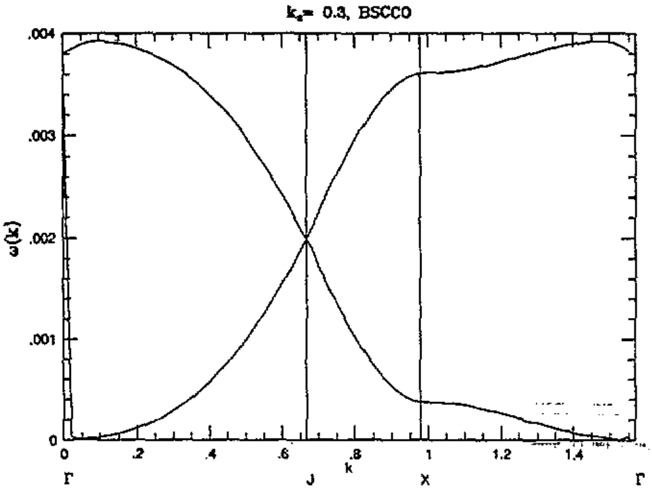

Figure 8. As figure 5, but at $k_z = 0.3$ for BSCCO.

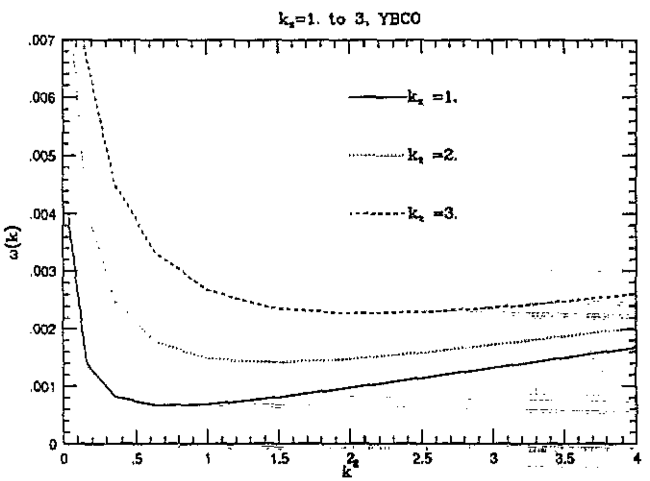

Figure 9. The transverse frequencies (in units of $B^2/4\pi$) as a function of k^2 for transverse momentum (k, k) at different values of k_z for YBCO.

To exhibit the behaviour of the transverse branch at finite wavevectors more clearly, we show in figure 9 the eigenvalues of this branch for different values of k_z (1, 2, 3) as a function of k^2 for $k_x = k_y = k$. After the rapid fall-off, the transverse branch is nearly linear in the transverse momentum squared. Its magnitude increases as k_z is increased. A similar set of curves is shown in figure 10 where the overall magnitude of k_z is decreased. (0.1, 0.2, 0.3) Because the magnitude of k_z is smaller, the shift in ω for different k_z is much smaller and the three curves at large q nearly lie on top of each other. Two similar sets of curves for BSCCO are shown in figures 11 and 12. Because Λ_2 is now much bigger, the shift as a function of k_z is much smaller in this case than that for YBCO.

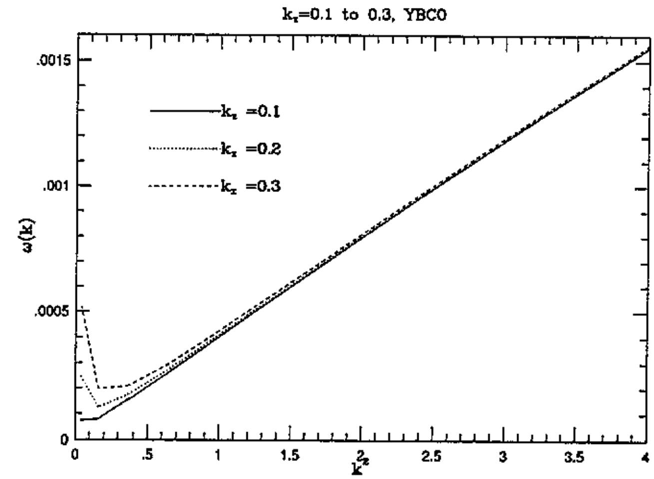

Figure 10. As figure 9, but at a smaller range of values of k_z for YBCO.

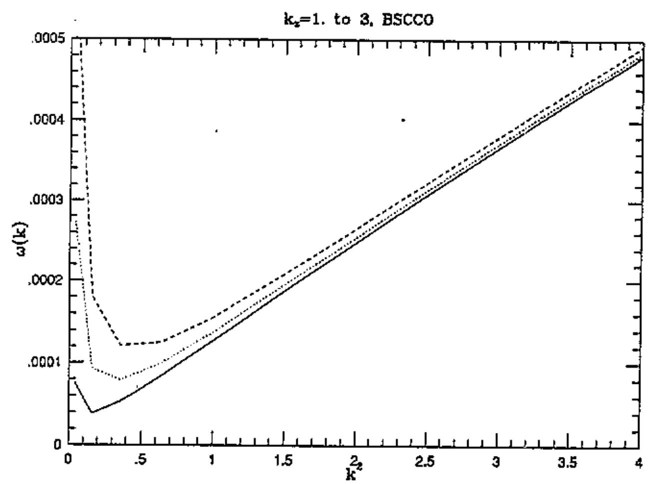

Figure 11. As figure 9, but at different values of k_z for BSCCO.

To emphasize the dependence on k_z, we show in figure 13 the transverse frequencies as a function of k_z for three different values of k_x. Expanding V^b as a power series of $(1 + \Lambda_1 k_z^2)/\Lambda_2 q^2$, we expect the slope of the curve to decrease as k_x is increased, as is shown in the figure. We note that this slope is much smaller than that at zero transverse wavevector, c_{44}. As expected, this slope is controlled by the mass ratio which determines Λ_2. On the other hand, the slope is not just the simple

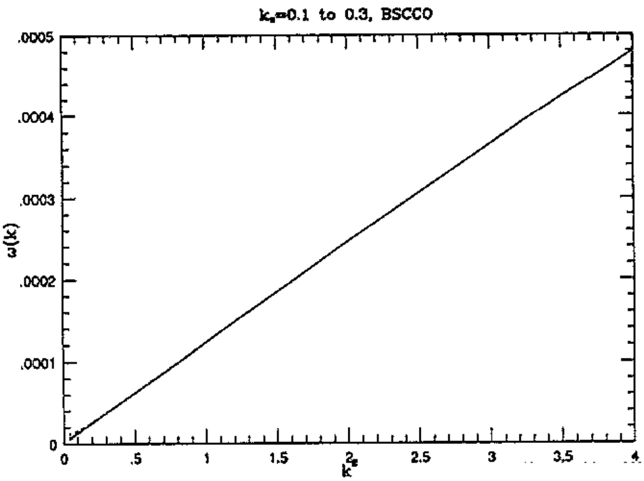

Figure 12. As figure 9, but at a smaller range of values of k_z for BSCCO.

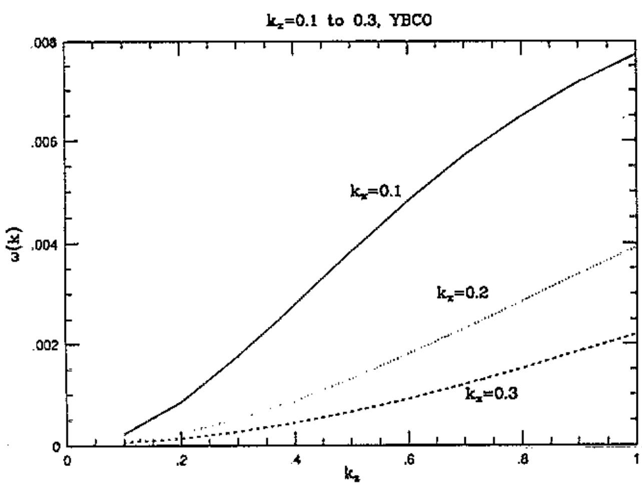

Figure 13. The transverse frequencies (in units of $B^2/4\pi$) as a function of k_z for different transverse momentum (k_x, k_x) for YBCO.

ratio M_z/M. We show the same dispersion over a much wider range in k_z in figure 14. As k_z is increased, the dependence on k_x is reduced. The dependence of the transverse frequencies on k_z for BSCCO is shown in figure 15. The magnitude of the frequencies are much smaller because Λ_2 is now much bigger.

The dependence of these normal frequencies on other physical parameters is what one expected. To illustrate, we show in figure 16 the 2D dispersion curves at $k_z = 0.3$ for BSCCO for a much smaller magnetic field of 100 G. Now the lattice spacing in comparison with the penetration depth is much larger. Thus the potential is shorter in range. The compressive branch now exhibits a much stronger dispersion.

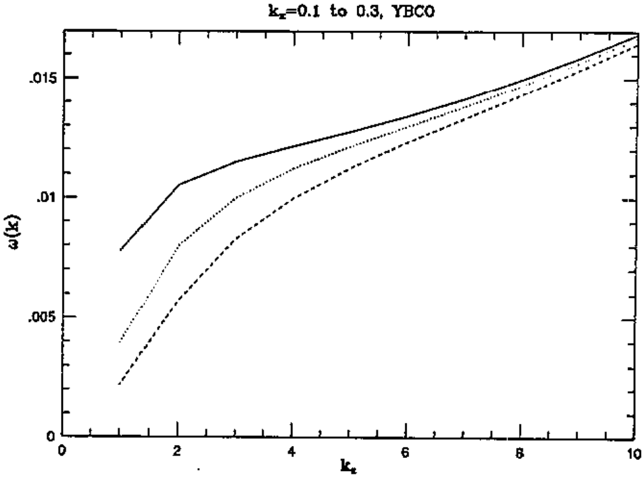

Figure 14. As figure 13, but for a larger range of k_z for YBCO.

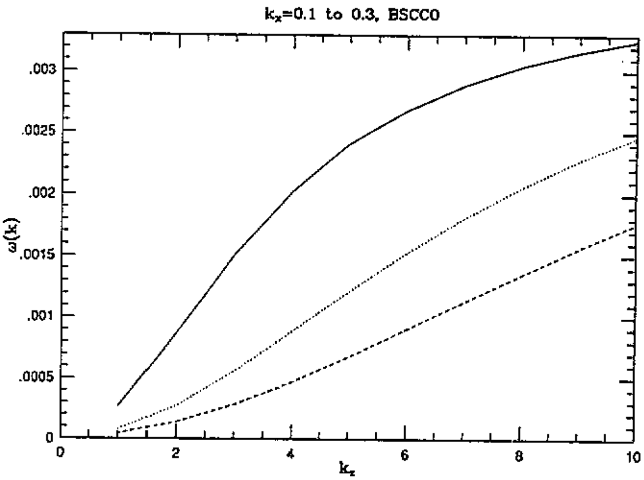

Figure 15. As figure 13, but for BSCCO.

4. Elasticity

The elastic coefficients c_{ij} are defined by

$$\Phi(k) = k_\alpha k_\beta[c_{11}(k) - c_{66}] + \delta_{\alpha\beta}[(k_x^2 + k_y^2)c_{66} + k_z^2 c_{44}(k)]. \qquad (4)$$

The elasticity for anisotropic flux lattices were recently studied by Houghton *et al* [2] from the Ginsburg–Landau equation and by Sudbø *et al* [1] from the London equation. In both these calculations, the elastic constants are calculated with the continuum approximation so that the summation over the reciprocal lattice Q of the flux lattice is replaced by an integral. In this paper, we evaluate these coefficients exactly. We found that at $k = 0$, the dependence of c_{44} on the magnetic field is well produced by the analytic formulae previously proposed. The difference and similarity with the results from the continuum approximation is highlighted in figures 16 to 18.

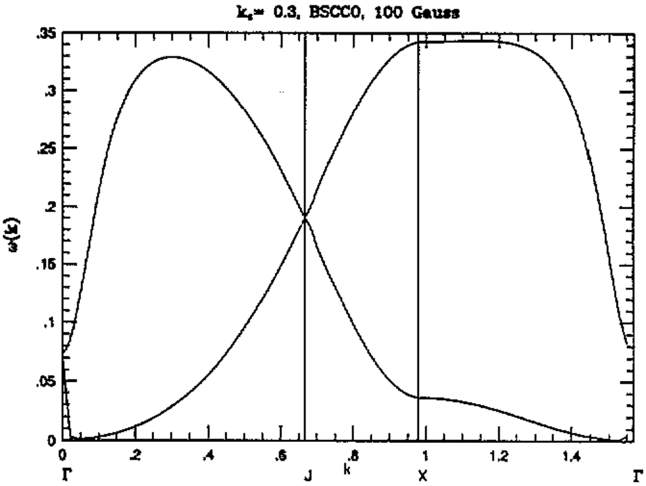

Figure 16. The normal mode frequencies (in units of $B^2/4\pi$) along symmetry directions in the 2D hexagonal Brillouin zone for $k_z = 0.3$ at B=100 G for BSCCO.

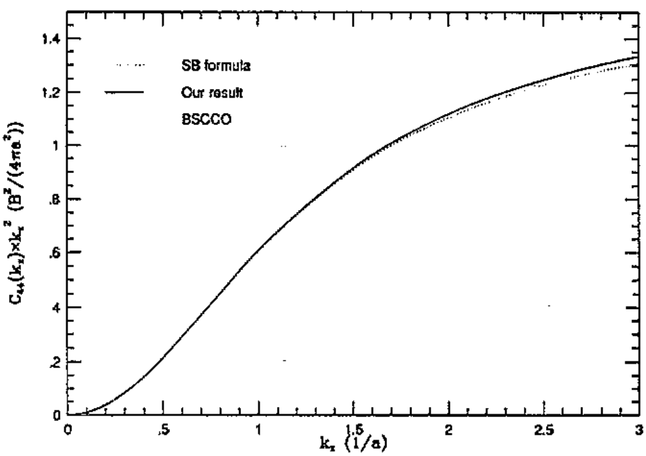

Figure 17. The elastic energy $c_{44}(k_z)k_z^2$ at high fields as a function of k_z $b = B/H_{c2} = 0.1$, $a = (2\Phi_0/\sqrt{3}B)^{0.5}$ is the flux lattice constant. Also shown are the results of [2].

In figures 17 and 18 we show $c_{44}(k_z)k_z^2$, which is a measure of the elastic energy, as a function of k_z at high field for BSCCO for two different ranges of k_z. There is some difference from the continuum approximation, at large k_z but it is quite small.

In figure 19 we show results for c_{66} at $k = 0$ as a function of the magnetic field. The difference between the continuum approximation and our result is also quite small for c_{66}.

The result in the previous section of the rapid drop in the shear mode eigenvalue as the transverse wavevector is increased can be interpreted as a substantial dependence of the shear modulus on the transverse wavevector. This fact is not discussed in previous work.

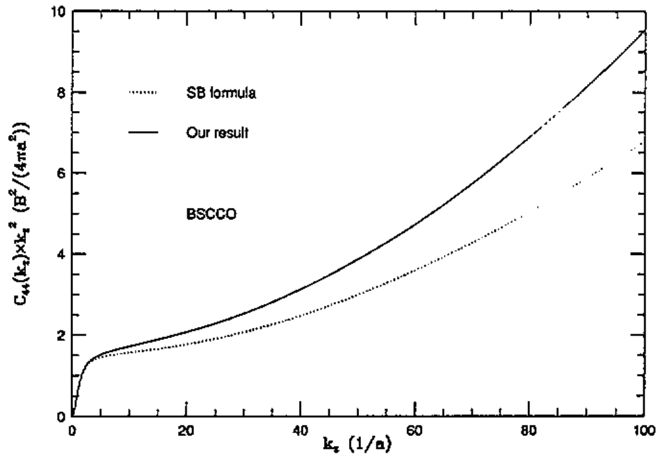

Figure 18. The elastic energy $c_{44}(k_z)k_z^2$ at high fields as a function of k_z over a larger range of wavevector. Also shown are the results of [2].

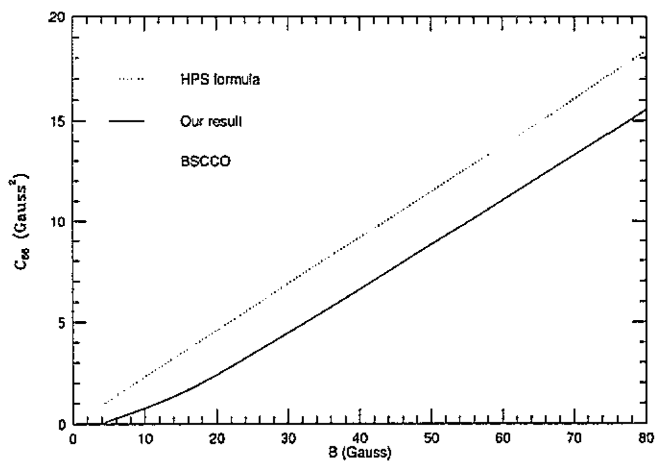

Figure 19. The elastic coefficient c_{66} at $k = 0$ as a function of the magnetic field B. Also shown are the results of [1] labelled as HPS.

5. Ewald sum

Direct evaluation of (1) is impractical because it is slowly convergent for large Q. To get a rapidly convergent result, we use the Ewald sum method where we rewrite the sum over Q in (1) into sum in real space and a sum in reciprocal space.

There are two kinds of terms involved in the summation, the first comes from the V_{zz} term in (1) and is given by

$$E_1 = \sum_Q \frac{(k+Q)_\alpha (k+Q)_\beta}{\Lambda_1^{-1} + (k+Q)^2} \exp[-\zeta(k+Q)_\perp^2].$$

The other one comes from the $V_{\alpha\beta}$ term and is given by

$$E_2 = \sum_Q \frac{(k+Q)_\perp^2 \delta_{\alpha\beta} - (k+Q)_\alpha (k+Q)_\beta}{(\Lambda_1^{-1} + (k+Q)^2)((\Lambda_1+\Lambda_2)^{-1} + (k+Q)_\perp^2 + \Lambda_1(\Lambda_1+\Lambda_2)^{-1} k_z^2)} \times \exp[-\zeta(k+Q)_\perp^2]$$

where we have used the identity $q_\alpha q_\beta = k_\perp^2 \delta_{\alpha\beta} - k_\alpha k_\beta$. E_1 can be obtained from the derivative with respect to r of the expression

$$\sum_Q \frac{\exp[\mathrm{i}(k+Q)_\perp \cdot r]}{\Lambda_1^{-1} + (k+Q)^2} \exp[-\zeta(k+Q)_\perp^2].$$

Using the identity $\int_0^\infty \mathrm{d}\epsilon\, \mathrm{e}^{-\epsilon x} = 1/x$, it can be written as

$$\sum_Q \int_0^\infty \mathrm{d}\epsilon \exp[-\epsilon(\Lambda_1^{-1} + (k+Q)^2) - \zeta(k+Q)_\perp^2] \exp[\mathrm{i}(k+Q)_\perp \cdot r] = I_1 + I_2.$$

Here $I_{1,2}$ is obtained by dividing the integration over ϵ into two parts from 0 to η and from η to ∞ for a suitable Ewald cut-off parameter η.

$$I_1 = \sum_Q \int_0^\eta \mathrm{d}\epsilon \exp[-\epsilon(\Lambda_1^{-1} + (k+Q)^2) - \zeta(k+Q)_\perp^2] \exp[\mathrm{i}(k+Q)_\perp \cdot r] \qquad (5)$$

$$I_2 = \sum_Q \frac{\exp[-\eta(\Lambda_1^{-1} + (k+Q)^2) - \zeta(k+Q)_\perp^2] \exp[\mathrm{i}(k+Q)_\perp \cdot r]}{\Lambda_1^{-1} + (k+Q)^2}. \qquad (6)$$

The sum over Q in I_2 converges very quickly. Now we transform the first summation to one in real space with the relation $\sum_R \exp(\mathrm{i}p \cdot R) = (2\pi)^2 n \sum_Q \delta(p+Q)$ where n is the density.

$$I_1 = \sum_R \int \frac{\mathrm{d}^2 p}{(2\pi)^2} \int_0^\eta \mathrm{d}\epsilon \exp[\mathrm{i}(k+p)_\perp \cdot (r+R) - \epsilon(\Lambda_1^{-1} + (k+p)^2) - \zeta(k+p)_\perp^2] \times \exp(-\mathrm{i}k_\perp \cdot R]).$$

The integration over p can be easily done and we get

$$I_1 = \sum_R \int_0^\eta \mathrm{d}\epsilon \frac{\exp\{-\epsilon(\Lambda_1^{-1} + k_z^2) - [(r+R)^2/4(\epsilon+\zeta)]\}}{4\pi n(\epsilon+\zeta)} \exp(-\mathrm{i}k_\perp \cdot R). \qquad (7)$$

The summation in R for I_1 is also rapidly convergent. Our purpose is thus accomplished.

The same procedure can be used to treat E_2. Instead of writing the formula as an integration over a single parameter ϵ, we have to introduce two auxiliary integrations and divide each integral into two parts. More precisely, define $A = \Lambda_1^{-1} + k_z^2$, $B = (\Lambda_1 + \Lambda_2)^{-1} + (M/M_z)k_z^2$, $f_1 = A + (Q+k)_\perp^2$, $f_2 = B + (Q+k)_\perp^2$; E_2 can be obtained from the derivative of

$$E_2' = \sum_Q \exp[\mathrm{i}(k+Q)_\perp \cdot r - \zeta(k+Q)_\perp^2]/(f_1 f_2).$$

This can be transformed to

$$E_2' = \sum_Q \int_0^\infty \int_0^\infty \mathrm{d}\epsilon_1\, \mathrm{d}\epsilon_2\ \exp[-\epsilon_1 f_1 - \epsilon_2 f_2 - \zeta(k+Q)_\perp^2] \exp[\mathrm{i}(k+Q)_\perp \cdot r].$$

Divide the integration into four parts depending on whether $\epsilon_{1,2}$ is larger or smaller than η. Only the term with both ϵ_1 and ϵ_2 less than η does not contain an exponential factor and hence is slowly convergent in Q space. This term (called J_1 below) is converted into a sum over R space. More precisely:

$$\begin{aligned} E_2' &= \sum_Q \left[\int_0^\eta \mathrm{d}\epsilon_2\ \exp(-\epsilon_2 f_2) + \exp(-\eta f_2)/f_2)\right] \\ &\quad \times \left[\int_0^\eta \mathrm{d}\epsilon_1 \exp(-\epsilon_1 f_1) + \exp(-\eta f_1/f_1)\right] \\ &\quad \times \exp[-\zeta(k+Q)_\perp^2] \exp[\mathrm{i}(k+Q)_\perp \cdot r] \\ &= J_1 + J_2 \end{aligned}$$

where

$$J_1 = \sum_Q \int_0^\eta \mathrm{d}\epsilon_2 \int_0^\eta \mathrm{d}\epsilon_1 \exp[-\epsilon_2 f_2 - \epsilon_1 f_1] \exp[-\zeta(k+Q)_\perp^2] \exp[\mathrm{i}(k+Q)_\perp \cdot r]$$

$$\begin{aligned} J_2 &= \sum_Q [\exp(-\eta f_1) + \exp(-\eta f_2) - \exp(-\eta f_2 - \eta f_1)] \exp[-\zeta(k+Q)_\perp^2] \\ &\quad \times \exp[\mathrm{i}(k+Q)_\perp \cdot r]/f_1 f_2. \end{aligned}$$

Now convert the Q sum into an R sum for the first term; we get

$$\begin{aligned} J_1 &= \sum_R \Bigg[\int_0^\eta \mathrm{d}\epsilon_2 \int_0^\eta \frac{\mathrm{d}\epsilon_1}{4\pi(\epsilon_1+\epsilon_2+\zeta)} \\ &\quad \times \exp\left(-\epsilon_2 B - \epsilon_1 A - \frac{(r+R)^2}{4(\epsilon_1+\epsilon_2+\zeta)} - \mathrm{i}k\cdot R\right)\Big/ n\Bigg]. \end{aligned}$$

Now change the variables of integration to $s = \epsilon_1 + \epsilon_2$, $t = A\epsilon_1 + B\epsilon_2$; we get

$$\begin{aligned} U/NL &= \sum_Q \frac{\exp[-\eta(\Lambda_1^{-1} + Q^2) - \zeta Q_\perp^2]}{\Lambda_1^{-1} + Q^2} + \sum_R \int_0^\eta \frac{\mathrm{d}\epsilon}{4n\pi(\epsilon+\zeta)} \\ &\quad \times \exp\left(-\epsilon\Lambda_1^{-1} - \frac{R^2}{4(\epsilon+\zeta)}\right) \end{aligned}$$

$$\Phi(k) = \frac{B^2}{4\pi\Lambda_1}(k_z^2 \phi_{\alpha\beta}^{(1)}(k) + \phi_{\alpha\beta}^{(2)}(k)) \tag{8}$$

$$\phi^{(1)}_{\alpha\beta}(k) = \sum_Q \frac{\exp[-\eta f_1 - \zeta(Q+k)^2_\perp]}{f_1}\delta_{\alpha\beta} + \sum_R \int_0^\eta \frac{\mathrm{d}\epsilon}{4\pi(\epsilon+\zeta)}$$

$$\times \exp\left(-\epsilon A - \frac{R^2}{4(\epsilon+\zeta)} - \mathrm{i}k\cdot R\right)\delta_{\alpha\beta} - \frac{\exp[-\zeta(Q+k)^2_\perp]\Lambda_2}{(\Lambda_1+\Lambda_2)}$$

$$\times \sum_Q \frac{(Q+k)^2_\perp \delta_{\alpha\beta} - (k+Q)_\alpha (k+Q)_\beta}{f_1 f_2}$$

$$\times \{\exp[-\eta f_1] + \exp[-\eta f_2] - \exp[-\eta(f_1+f_2)]\}$$

$$-\frac{1}{n}\sum_R \int_0^{2\eta} \frac{\mathrm{d}s}{4\pi(s+\zeta)} g(s)\left[\left(\frac{1}{2(s+\zeta)} - \frac{R^2}{4(s+\zeta)^2}\right)\delta_{\alpha\beta}\right.$$

$$\left. + \frac{R_\alpha R_\beta}{4(s+\zeta)^2}\right]\exp\left(-\frac{R^2}{4(s+\zeta)} - \mathrm{i}k\cdot R\right)$$

$$\phi^{(2)}_{\alpha\beta}(k) = \sum_Q \frac{(k+Q)_\alpha (k+Q)_\beta \exp[-\eta(\Lambda_1^{-1} + (k+Q)^2) - \zeta(Q+k)^2_\perp]}{\Lambda_1^{-1} + (k+Q)^2}$$

$$-\sum_Q \frac{Q_\alpha Q_\beta e^{-\eta(\Lambda_1^{-1}+Q^2) - \zeta Q^2_\perp}}{\Lambda_1^{-1} + Q^2}$$

$$+\frac{1}{n}\sum_R \int_0^\eta \frac{\mathrm{d}\epsilon}{4\pi(\epsilon+\zeta)} \exp\left(-\epsilon(\Lambda_1^{-1} + k_z^2) - \frac{R^2}{4(\epsilon+\zeta)} - \mathrm{i}k\cdot R\right)$$

$$\times \left(\frac{-1}{2(\epsilon+\zeta)}\delta_{\alpha\beta} + \frac{R_\alpha R_\beta}{4(\epsilon+\zeta)^2}\right) - \frac{1}{n}\sum_R \int_0^\eta \frac{\mathrm{d}\epsilon}{4\pi(\epsilon+\zeta)}$$

$$\times \exp\left(-\epsilon\Lambda_1^{-1} - \frac{R^2}{4(\epsilon+\zeta)}\right)\left(\frac{-1}{2(\epsilon+\zeta)}\delta_{\alpha\beta} + \frac{R_\alpha R_\beta}{4(\epsilon+\zeta)^2}\right)$$

where the function g is defined as

$$g = \begin{cases} \dfrac{1}{A-B}\exp(-Bs)1 - \{\exp[-(A-B)s]\} & \text{if } s \leqslant \eta \\ \dfrac{1}{A-B}\exp[-As + (A-B)\eta]1 - \{\exp[(A-B)(s-2\eta)]\} & \text{if } \eta \leqslant s \leqslant 2\eta. \end{cases}$$

This is the main result of the present paper. Despite its complicated appearance, the integration involved in the above expression are well defined and rapidly convergent. We have evaluated it numerically. The Ewald parameter η is chosen to be n/π so that the range in Q and R is comparable. The integral over ϵ is evaluated with a simple Simpson's rule subroutine.

6. Conclusion

In conclusion, we have investigated the normal modes of vibration of the flux lattice. We found two normal modes corresponding to the shear and the compression of the lattice. The frequencies of these two are usually very different from each other at moderate magnetic field strengths. Because the penetration depth is much larger than the lattice spacing the potential is long range, the compressive mode behaves like a plasma oscillation. At zero momentum the exciations are gapless because the potentially is eventually exponential in character at large distances. As the magnetic field is decreased, the potential becomes less long range and the compessive mode exhibits a stronger dispersion.

At a finite z wavevector we found that the transverse frequencies drop off rapidly as the transverse wavevector is increased. The wavevector range in which this transition takes place is controlled by the mass anisotropy.

Much of recent work on flux lattices are based on elasticity theory. Thus it is important to study them in detail. We have provided here expressions for the elastic modulus that are rapidly convergent and hence is useful numerically. Our result can be significantly different from previous results obtained using the continuum approximation.

Acknowledgments

We thank Drs Sudbø and Brandt for sending us their papers prior to publication.

References

[1] Brandt E H 1990 *Physica* B **165/166** 1129
Sudbo A and Brandt E H 1991 *Phys. Rev. Lett.* **66** 1781

[2] Houghton A, Pelcovits R and Sudbo A 1989 *Phys. Rev.* B **40** 6763